Photonic properties of hybrid colloidal crystals fabricated by a rapid dip-coating process

ARTICLE *in* PHYSICAL CHEMISTRY CHEMICAL PHYSICS · JUNE 2011

Impact Factor: 4.49 · DOI: 10.1039/c0cp02517h · Source: PubMed

PCCP

Cite this: *Phys. Chem. Chem. Phys.*, 2011, **13**, 10681–10689

www.rsc.org/pccp

PAPER

Photonic properties of hybrid colloidal crystals fabricated by a rapid dip-coating process†

C. Deleuze,[a] B. Sarrat,[a] F. Ehrenfeld,[a] S. Perquis,[b] C. Derail[a] and L. Billon*[a]

Received 12th November 2010, Accepted 22nd February 2011
DOI: 10.1039/c0cp02517h

The enhancement of the capillarity fabrication of well-ordered two-dimensional (2D) and three-dimensional (3D) opal photonic crystal is described herein. The quality enhancement and the reduction of the fabrication time are improved by using core@soft adhesive shell (Silica@PolyButylAcrylate) particles dispersed in an organic solvent with a high boiling point. The hybridization by an elastomeric corona polymer, grafted from the SiO_2 surface, has offered adhesive properties naturally tunable by changing the polymer state from a solvated to a dry one. Such properties involve drastic changes of the self-assembly behavior and qualities. Their use, as elementary building blocks, for colloidal crystal fabrication have required a high withdrawal rate (up to 4000 μm s^{-1}), *i.e.* involving a three order of magnitude reduction in time compared to a classic vertical deposition method (1 to 10 μm s^{-1}) and a good control/prediction of the coating thickness can be tuned by varying the withdrawal rate and the particle concentration. In addition, an analysis of the 2D synthetic iridescence of the hybrid photonic crystal was performed under white light, revealing the adhesive shell bridge influence on the dissipation energy of cracks linked to the crystal quality and the photonic properties.

Introduction

The assembly of nano or micro particles into a material with long range organization has always attracted great scientific interest.[1] Combining billions of nanometric spherical particles into one colloidal crystal, also called 'opal' due to its similarities with the natural gemstone, has provided unique expected properties. Since Yablonovitch in 1987 who theoretically presented the existence of a photonic band gap for periodic dielectric materials, particular attention has been focused on colloidal crystal optical applications.[2] As one of the photonic band gap (PBG) class of materials, colloidal crystals can confine and propagate light in controlled directions with few losses and so they are developed for optics, telecommunications and the computer industry as chemical sensors,[3] low threshold lasers,[4] non-reflecting coatings,[5] switches,[6] or for wave guiding.[7] More recently, this class of materials has been used as template for various chemical porous materials or 'inverse opal' also used in optical or catalyst devices.[8]

The traditional approach to form such periodic material is through micro-fabrication methods,[9] such as the patterning through photolithography,[10] or holography processes,[11] laser etching,[12] chemical mechanical planarization,[13] or nanorobot-assisted manipulation.[14] Even if these approaches have been undertaken to produce a perfectly spherical building blocks, few of them are suitable to be used as real methods for upscaling as they are time consuming. In contrast, everyone agrees that colloidal assembly is a simple way to consider the fabrication of rapid PBG on large substrate. Many methods have been elaborated to coat and organize particles onto surfaces.[15,16] The first method is based on the application of an external field as a driving force to self-organize the particles. The most natural process is the sedimentation method based on gravity effect.[17] Recently, sedimentation of colloidal crystals in solution was illustrated by Ohno *et al.* using core@shell particles of silica Si@PMMA (PolyMethyl MethAcrylate).[18] The particles are left to settle in a mixed solvent medium until the formation of crystal. Then, the solvent is removed by thermal treatment. The nucleation and the layer by layer assembly, in a so-called colloidal epitaxy,[19] are influenced by the gravity effect (Stokes' law), the Brownian motion, the crystal nucleation and expansion depending on colloidal interactions and concentration. The weak points of this technique are the perfect adjustment of the experimental conditions to give the number of self-assembled layers required, and the long process time which can last up to months. To enhance the process, control of the sedimentation natural parameter, other external parameters such as electric field, magnetic field, and gas flow were used by Ristenpart *et al.* who showed the change of triangular to square-packed arrays, depending on the

[a] *Université de Pau et Pays de l'Adour, IPREM/UMR 5254/Equipe de Physique et Chimie des Polymères, Hélioparc, 2 avenue Angot, 64053 Pau Cedex 9, France. E-mail: laurent.billon@univ-pau.fr*
[b] *ColorDIMENSIONS, Hélioparc, 2 avenue Angot, 64053 Pau Cedex 9, France*
† Electronic supplementary information (ESI) available. See DOI: 10.1039/c0cp02517h

frequency applied.[20] The 'evaporation-induced self assembly' is the second and the most developed method, based on capillarity effect, to assemble colloidal particles well over a large surface. Unlike the spin coating method, the capillarity effect is based on the surface tension contrast between a liquid with particles and a dipped solid surface.[21] Among all available colloidal array formation methods found in literature, two ways are distinguished due to their dynamic self-assembly effects. Both of them consist of withdrawing vertical substrates at a constant rate as for dip coating,[22] or Langmuir Blodgett methods,[23] and to evaporate the solvent as for the vertical deposition method (VD).[24] More recently, Shimmin *et al*. have proposed, for 1 μm sulfate polystyrene beads, to combine the two ways by explaining the VD coating as a Langmuir–Blodgett coating only governing by particles behavior on air-solvent interface when the evaporation rate exceeds the sedimentation velocity.[25] The VD method, presented first by the Colvin's group, is perhaps the most used technique notably for capillarity assembly because of their conventional tool set up.[24] Nevertheless, two inherent issues remain (1) the increase of the particle layer number with time and (2) the particles sedimentation because of the gradual solvent evaporation over a long period of time. The Wong *et al*. process, which generates a constant particle flow by heat convection movement, has been used to try to limit the sedimentation effects.[26] The inherent thickness fluctuations described by Shimmin[25] and The[27] were further developed by Lozano *et al*. into a model that takes into account the stick-slip contact line motion caused by the competition between surface tension forces.[28] Despite its simplicity, the VD method was not the first one developed. Indeed, the VD method is derived from the dip coating method (DP), for which the first apparatus was developed during the 1940s. In 1943, Flemming *et al*. presented a dip coater that formed reproducible thin layers with a withdrawal rate of 8 to 17 $\times$ 10^{-4} m s^{-1}.[29] Since then, the DP has always attracted much attention, but it's only in 1968 with the Stöber process and the synthesis of silica colloids that the dip coater has gone up in value.[30] Among all the multiple studies on the subject, the true breakthrough was in 1996 with Nagayama and Dimitrov who proposed a primary model based on material flux balance in the field of colloidal assembly (eqn (1)).[22]

$$k = \frac{\beta.h.j_e}{0,605.\Phi.U}\frac{\varphi}{(1-\varphi)} \quad (1)$$

where k is the number of layers, U is the withdrawal rate, φ is the particle volume fraction, j_e is the solvent evaporation rate, Φ is the diameter of particles, h is the meniscus height, and β is a ratio between the particle and the solvent velocity (generally $\approx$ 1). The process was developed using 1 vol% PolyStyrene (PS) particles stabilized by surfactants, at low rate from 0.1 to 30 μm s^{-1} equal to the solvent evaporation to ensure a steady-state growth. Also confirmed for the same rate order by Sato *et al*.,[31] the main conclusion deduced from this equation is that the number of layers seems to increase with a decrease of the rate. This consideration is a real issue when attempting to form multilayers in short time. For instance, 45 min is calculated from the effective rate range as the time needed to assemble a colloidal monolayer on a small classic microscope slide. Industrially, the long time taken by this process is a current issue. For ensuring the colloidal assembly durability, the processing time has to be reduced. Nevertheless, with the model and the range of manufacturing process present in the Nagayama experiments, the DP method is limited. To remediate to this issue, we present here a new view on the DP method with a range of higher withdrawal rates, able to reduce the assembly time by 200 times, *i.e*. reducing time to assemble a monolayer on a microscope glass slide from 45 min with a classical method to only 14 s with our improved method. We changed the basis of the process by tuning the set up conditions and the complexity of the core@soft shell nanoparticles as an elementary adhesive building block. We followed the evolution of the coating behavior by proposing new state equations. A last part is dedicated to the observation of the photonic and spectroscopic analysis of the colloidal crystals thus obtained.

Experimental

Silica particles synthesis

Monodispersed Silica SiO_2 spheres (Si) were synthesized by a bottom up Stöber/Nozawa process.[32] Defined concentrations of ethanol (EtOH), ammonia and water are mixed in a 250 mL two necked round bottom flask. A solution of TetraEthoxy-OrthoSilicate (TEOS) and EtOH is added according to two methods, *i.e*. either it is added in one go, or it is added continuously through a pump syringe at a constant addition rate. The mixture is stirred at 200 rpm for 12 h after completion of the addition step to reach the complete reaction. The formation of silica particles of less than 300 nm is highlighted by the apparition of a soft blue color due to Rayleigh diffusion. Above this diameter, the color becomes white as predicted by the diffusion efficiency theory.

Core@soft adhesive shell nanoparticles synthesis

A nitroxyde mediated initiator was first synthesized by the previously presented '*in situ* thermo-dependant trapping of carbon radicals' process which described the addition of an 2-Methyl-2-[*N*-tertbutyl-*N*-(diethoxy-phosphoryl-2,2-dimethyl-propyl)aminoxy]propionic acid (MAMA) with trimethoxy silyl propyl acrylate (TPMA) to initiate synthesis of Poly(Butyl-Acrylate) PBuA.[33]

The core@shell hybrid particles experimental procedure was extensively described by our group elsewhere.[34,35] The Si@PBuA colloids were finally dispersed in N-Methyl Pyrrolidinone (NPY).

Self-assembly of the core@soft shell nanoparticles as elementary building blocks for colloidal crystal fabrication

A glass slide (75 $\times$ 25 mm) was previously treated by a piranha solution containing 70 vol% sulfuric acid and 30 vol% hydrogen peroxide. The substrate was dipped in a Si@PBuA dispersion with a defined wt%. The dispersion was contained in a 50 mL flask under slow stirring (50 rpm) to avoid the aggregates formation and sedimentation of large particles over a long time. After waiting for one minute, which is necessary to reach a stable equilibrium, the substrate is withdrawn from

the media at a constant rate. We have designed and set up a Dip coater system to prepare various films from liquid solutions over areas as large as 5 cm^2 (2 cm × 2.5 cm). The originality of our home-made material was to provide programmable rotation of the tilt angles from 0 to 30° with a range of vertical lengths up to 100 mm. Profile dipping was then accomplished by moving the rotational and translation DC motor control, at different rates, into a stationary dip tank. DC motor control of the dipping arm and rotation axes provided smooth motion of the substrate. The rate of the substrate was imposed by mechanical arm linked to a step-by-step motor with a rate range from 1 to 4000 μm s^{-1}. Home-made software has been programmed to control the deposition, immersion rate, rotation angle, drying period and finally the number of dip cycles. The material was dried horizontally at room temperature. Environmental Scanning Electron Microscope (ESEM) observations were performed by using an electroscan E-3 and Transmission Electron Microscopy was performed by using a JEOL JEM-2000 FX with an accelerating voltage of 200 kV at room temperature.

Goniometric characterization

The spectroscopic data have been instantaneously acquired in reflection by a spectrogonio-colorimeter developed by ColorDIMENSIONS®. This system was developed from a matrix CCD video coupled with 28 optical fibers which defined a circular plan from 3 to 84 degrees for the analyses (Fig. ESI-1 in electronic supporting information†). The incident lighting was provided by an OSRAM XBO 150 OFR Xenon source filtered in UV-A, B and C. All the detectors were automatically calibrated to record simultaneous captures of light on the source and sample on a PTFE white background. The acquisition time has been fixed to assure better reproducibility.

Laser diffraction pattern

A 3 mW, 637 nm, red diode laser beam was applied to the colloidal crystal sample at normal incidence. The 2D diffraction symmetry was observed by transmission with a home-made setup. The diffraction pattern was captured by a SONY® IEEE 1394 CCD camera through a macro telecentric lens.

Results and discussion

Building blocks based on core@soft adhesive shell particles

The silica particle SiO_2 synthesis was conducted by a bottom up Stöber process.[30] This process was improved by the use of the constant addition growth which allows the synthesis of monodisperse particles of 1μm diameter (Table ESI-2 and Fig. ESI-3 in electronic supporting information†).[32]

As we have recently described, core@soft shell nanoparticles exhibiting very smooth and homogeneous surfaces can be synthesized by Surface Initiated Nitroxide Mediated Polymerization, so-called SINMP. By this process, the PBuA shell thickness can be controlled by the tailoring of the grafting density or/and the molecular weight MW.[34] Here, a shell thickness was obtained around 45 nm, corresponding to a grafting density of 0.25 molecule nm^{-2} and to a MW of 85 000 g mol^{-1} (Fig. 1). The MW was calculated after degrafting procedure as described by Parvole *et al.*[35]

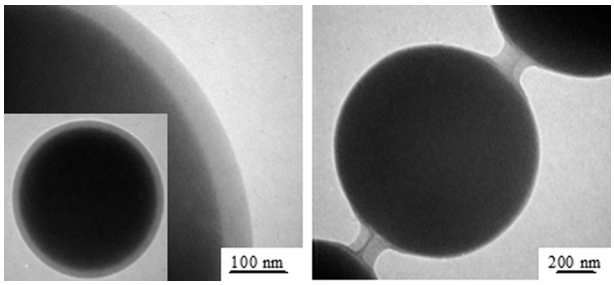

Fig. 1 TEM images of core@soft shell spherical hybrid particle and fibril due to the strong adhesive interactions between PBuA soft shells (Silica core@soft PBuA shell, 1 μm@45 nm).

The grafting density is sufficiently high to present a so-called 'high density brush' behaviour. Moreover, the intrinsic PBuA behaviour as a sticky polymer was described as an important key parameter to tune and control the self-assembly of such elementary adhesive building blocks.[34,36] For the first time, we can herein observe, the adhesive and cohesive behaviour of the PBuA layers in the contact area where elongation of the elastomeric PBuA brushes is described as a fibrillation (Fig. 1 right). At this stage, this last point is not totally elucidated and the understanding of such a behaviour is still underway. An alternative explanation is that the adhesion between particles could also be due to strong attractive interactions between brushes induced by the brushes interpenetration.[37] It is expected that a high value of molecular weight between entanglements M_e facilitates the formation of fibrils which dissipate more energy and thus lead to better adherence properties.[38] PBuA exhibits a high M_e[36] and we have observed on our system that fibrillation appears when the PBuA is entangled *i.e.* when the molecular weight of the grafted chains is higher than 2 times molecular weight between entanglements of PBuA macromolecular chains.

Self-assembly of the elementary particles

Among the conceivable applications for the colloidal crystal, at least a few of them are now available because the elementary building blocks can now be assembled in a less time consuming process. The aim of this study was to provide an easy and rapid method to self-assemble particles into colloidal crystals and characterize them. During our preliminary experiment, we found that the coating thickness is proportional to the withdrawal rate while one can expect the opposite. To understand this change of behaviour, experimental results were compared to theory by using the Landau–Levich eqn (2) which describes the thickness of the meniscus h with the withdrawal rate U, the volumic mass ρ, the dynamic viscosity η, the gravitational constant g and a non-dimensional number Ca which defined the balance between the gravitational effect and the capillarity effect for a Newtonian fluid (eqn (2)).

$$h = 0.944(Ca)^{1/6}\left(\frac{\eta U}{\rho g}\right)^{1/2} \quad (2)$$

Even if the Nagayama method framework was not applicable in our case, his five described rules remained true according to our observations.[22] The two first rules govern the state of particles.

During the DP process, the particles have to be monodisperse, stable and suitable to slip along the substrate. In case of absorption, an amorphous phase on the sample top could be produced. For this reason, we employed monodisperse core@shell hybrid particles stabilized by a homogeneous adhesive corona based on PBuA elastomer. The shell maintained the dispersed character of the core@shell particles by the polymer corona swelling and thus avoiding the use of surfactants as chemical dispersant. In this case, the interaction between the substrate (glass slide) and the particles is modified from that of a hydrophilic particle to that of a hydrophobic particle, limiting Van der Waals (VDW) interactions. Indeed, the solvated core@shell hybrids behave following the Derjaguin-Landau-Vervey-Overbeek (DLVO) potential. Besides highly charged colloidal spheres, the particles behaviour is governed by two terms: the short range steric repulsive interactions and the long range attractive VDW interactions.[39] A soft stirring convection of the dispersion was applied between experiments to avoid long term sedimentation.

The second interest of the PBuA shell concerns its ambivalent sticky properties in solvent and in air. Indeed, the swollen hybrid particles remain non-sticky, like hard spheres, which allows the particles to slip along the substrate during the meniscus feed. But during the solvent evaporation step, the adhesion character of PBuA becomes more and more important, until reaching a very sticky behaviour due to a low elastic intrinsic elasticity. The sticky behaviour is expected to have a strong influence on the self-assembly behaviour (i) through the strong particle–substrate interactions but also (ii) by attenuating the violent evaporation effect of the capillary bridge on particles through the rupture energy dissipation, observable by the formation of fibrils or "bridges" instead of crack formations (Fig. 1 and Fig. 2). Using a simple hard sphere or polymer colloid as building blocks would not provide such interesting materials. By choosing a core@shell hybrid as elementary adhesive building blocks, we achieved one hybrid material combining the properties (i) a simple/mono block to self-assemble and (ii) a sticky behaviour effect to enhance adhesion between particles/particles and substrate/particles.[34] A similar idea was described concerning inter-particle adhesive bridges in order to increase crystal quality,

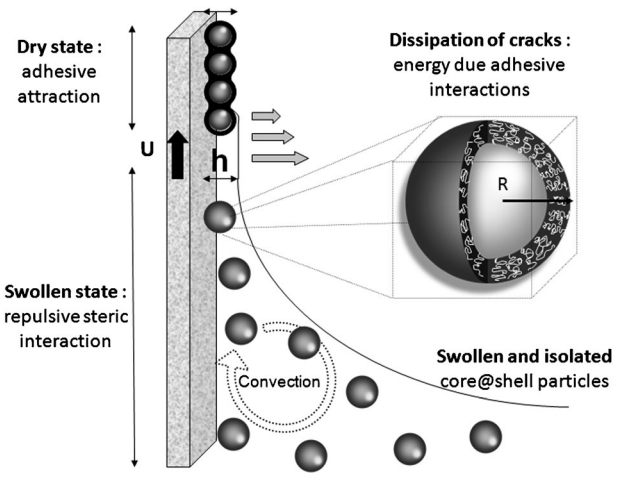

Fig. 2 Grafted adhesive shell influence on the Dip Coating process.

but using a different approach.[40] In our case, we suspect interparticular interactions tuning between solvated and dry states, *i.e.* a steric repulsion and an adhesive attraction, respectively (Fig. 2).

The last 3 rules concern the solvent choice. The solvent has to (i) evaporate moderately from the surface (ii) entirely wet it to form a meniscus and finally (iii) present a meniscus thickness with the same size order as the particle diameter. We observed for a low de-wetting solvent (EtOH + NH_4OH), the formation of impending droplets on the non dried area when the meniscus broke up, reducing the quality of the final sample. Also, in this specific range of rate and concentration, the meniscus thickness was estimated to be below the diameter of the particle. As a consequence, holes and cracks were observed in the array and sometimes formation of lines that could be explained as a stick-slip behaviour already described.[27,41] The last series of experiments were carried out on various solvents. We observe for low boiling point solvents (THF, Acetone, and EtOH), that the evaporation rate was too fast to support the particles self-assembly. Finally, we decided to choose a solvent with a higher boiling point to avoid the aggregation on defects and also to decrease the surface tension during the capillarity bridge evaporation, which often generated rupture cracks. The non-dimensional Capillarity number Ca can be developed as following in eqn (3) where γ and η are the surface tension and the viscosity of the solvent, respectively.

$$Ca = \frac{\eta U}{\gamma} \quad (3)$$

The number Ca defines the balance between the gravitational and the capillarity effects. If $Ca < 2.10^4$, the capillarity forces regulate the system and the gravitational forces are therefore neglected. Such case theoretically means that the liquid behaviour is not disturbed by the horizontal or vertical approaches of the sample. In order to optimize the system, the capillarity number was chosen as high as its limit value by choosing a higher withdrawal rate. To correspond to the higher value of Ca and to be suitable with the various rules previously described, the *N*-Methyl Pyrrolidinone (NPY) solvent has been chosen. This organic solvent has a particularly high boiling point of 220 °C and an interesting good wetting behaviour on glass substrates. Indeed, it shows a high surface tension of $\gamma = 40.8$ mN m^{-2} and a low viscosity $\eta_0 = 1.7 \times 10^{-3}$ Pa s^{-1}, two parameters required to achieve a high withdrawal rate. In the next part, the viscosity of the dispersed system η was dictated by the Einstein law: $\eta = \eta_0 + 2{,}5\varphi$ where φ is the volume fraction of particles.

Rapid tailoring of the coating thickness by control of the particles layers number

The decrease of the process time is a current industrial issue for large area fabrication. Nevertheless, the rate, the quality and the extension process are not the only aims to take into account. Indeed, the originality of colloidal crystal array performance compared to the other approaches is related to the ability to control the number of layers produced and their cohesion. Then, being able to provide a large range of numbers of layers is also a criterion of choice. For instance, colloidal

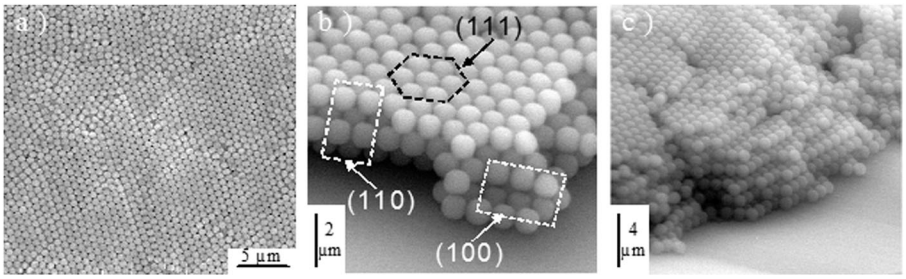

Fig. 3 Face Centered Cubic *fcc* ESEM observations of a top view multilayer (a), a side view of (111), (110) and (100) plan of 3 stacked layers (b) and side view of 8 stacked layers (c) (from left to right, respectively).

crystals for stop band filter applications require a control of the reflectance intensity function of the number of stacked layers.

So far, to achieve colloidal arrays from a monolayer to a multilayer with high rate, we based our work on a transformed Landau–Levich relation. We thus defined a cubic volume which determines the solvated sphere volume in a good solvent in order to simplify this approach. The thickness of the meniscus is divided by the number of solvated particles able to diffuse in this latter, which finally provide the expected number of self-organized layers, *i.e.* k (eqn (4)) where Φ is the diameter of one particle.

$$k = \frac{1.17}{\sqrt{\rho g}\Phi}\left[\frac{\varphi(\eta U)^2}{\sqrt{\gamma}}\right]^{1/3} \quad (4)$$

The volume fraction φ and the speed U were the two parameters easily tunable for the coating thickness modification. The development of a real monolayer is less flexible. Indeed, due to the fact that an external view is not conclusive enough to discern stack defects, good quality multilayers are, at first, more achievable than monolayers. So, some specific set-up conditions were developed for a stack control. As a view from above was not efficient to determine the number of layers experimentally, these analyses were performed with the sample on its side or on an area that had been scratched (Fig. 3).

The face centered cubic (*fcc*, ABCABC...), the hexagonal closed packed (*hcp*, ABAB...) and the randomly packed were the low-energy structures considered for colloidal crystallization. In case of non-interacting hard spheres, a low difference of entropy energy between *fcc* and *hcp* could explain the structuring preference for the *fcc* structure as illustrated in this study in Fig. 3(a).[42] The total presence of 74% packing density *fcc* on the crystal is called into question in the literature notably by the highlight of *hcp* or other transition structures investigated in the inner array.[43] The major (111) plan presented on top of the crystal leads the predictable diffracting properties. The presence of (110) and (100) plans is localized on the material side (Fig. 3(b)).

Additionally, in Fig. 3(a), the presence of so-called "fuzzy lines" is also observed as already described by Nagayama *et al.* Such behaviour is explained as being a consequence of the coating rate increase. Easily comparable to the grain boundary characteristic of metallic component, the "fuzzy lines" presence provides information on the default density but also removes the idea of the presence of deep fractures disturbing the structure.[22]

The number of layers formed is not infinitely extensible notably because of the two tunable parameters limits. In the case of rate U, the capillarity number and so the gravitation effect have a crucial influence. Indeed, imposing too a high rate involves surface dewetting and meniscus rupture. In the present study, the experimental withdrawal rate was found to be limited at 4000 µm s^{-1} which in fact corresponds well to the limit capillarity number value and the non-neglected gravitational force effect on the meniscus. Moreover, a high concentration of particles φ in the meniscus seems to disturb the array formation kinetics through the increase of the particle aggregates or by the decrease of the particle mobility. For high concentrations, the fabricated samples present a white scattering color corresponding to the increase the presence of defects. In consequence, an upper limit of the particles concentration φ was fixed to 18 vol% to reach the targeted number of layers.

We can theoretically target a higher number of layers by tilting the dip coater arm at various angles keeping the φ constant. As already described by Park *et al.* for the VD method, carrying out experiments under titled angles involves a change of the meniscus thickness.[44] The coating thickness on the superior face of the substrate tends, consequently, to increase and the thickness decreases on its interior face. Another way to self-assemble a high number of layers is the multiple coating method which is derived from the Langmuir–Blodgett process. In fact, the issue of particle diffusion in solution is a limiting factor for the following dip. The adhesive character of the polymer and the high rate used allow us to avoid it. Indeed, a stack of 8 layers can be obtained from the 3 stacked layer colloidal crystal (Fig. 3(b)) by two successive dips (Fig. 3(c)).

The possibility to form a multilayer with different particle sizes is interesting when dedicated to the formation of resonant photonic states inside the forbidden gap. Indeed, in this case the main idea is to form colloidal arrays with controlled defaults by insertion of a particle layer with smaller diameter as described by Ravaine *et al.*[45]

Nevertheless in our case, the multiple dip coating involves the creation of materials with a slightly worse final quality but presenting a higher layers number than this one predicted by the model for a simple dip. From our point of view, the repetition of self assembling on a coated substrate modifies the surface tension affinity of the solvent/substrate couple and

Table 1 Experimental conditions for colloidal crystals fabrication with high rate dip coating

Series	φ (%)	U (mm s^{-1})	h (μm)[a]	Ca (10^{-4})	k_{est}	k_{exp}
A1	15	4	6.8	2.2	3.0	3.0
A2	15	3	5.7	1.6	2.5	2.0
A3	15	1	2.7	0.5	1.2	1.0
A4	15	0.5	1.7	0.3	0.7	hole
B1	25	3	6.1	1.8	3.0	3.0
C1	3	3	5.0	1.3	1.4	1.0
C2	3	4	6.0	1.8	1.6	1.0

[a] The height h was calculated from the Landau-Levich equation $h = 0.944(Ca)^{1/6}\left(\frac{\eta U}{\rho g}\right)^{1/2}$.

disturbs the self-assembly process due to the micro-roughness and substrate chemical nature.

We notably focused on the prediction of the number of layers by targeting the development of a monolayer with a time consuming decrease of the protocol. The first approach was to coat material at higher φ and U in order to stay at the limit of the neglected gravitational regime. The experimental series (*A*) to (*C*) were carried out to confirm the model accuracy. The set up conditions are summarised in Table 1, for a colloidal crystal area as large as 20 × 25 mm.

Also presented in Fig. 4 and ESI-4† (magnified), the withdrawal rate modifies the number of layers with a good accuracy with the model. The monolayer state is reached at 1 mm s^{-1} with a *Ca* close to its limit (entry A3 in Table 1). Under this value, the array is surrounded by holes corresponding to a lack of particles. This state is illustrated by the value k_{est} less than 1 which means by a physical disruption of the meniscus feed.

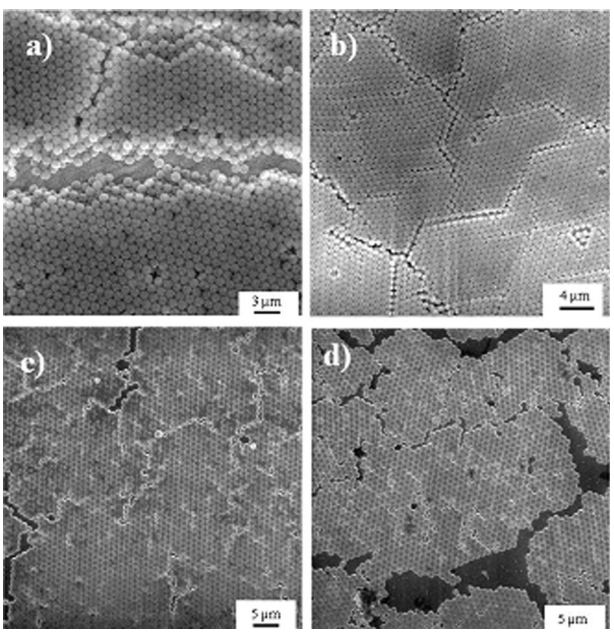

Fig. 4 ESEM observations after dip-coating deposition for a 15 vol% solution of hybrid silica particles with various withdrawal rates (a) 3 layers at 4 mm s^{-1} (entry A1 in Table 1), (b) 2 layers at 3 mm s^{-1} (entry A2 in Table 1), (c) 1 layer at 1 mm s^{-1} (entry A3 in Table 1) and (d) hole apparition at 0.5 mm s^{-1} (entry A4 in Table 1).

The effect of particles sedimentation is finally neglected for diameters around 800 nm. Compared with the sedimentation method, our process is too fast to be influenced by the sedimentation effect. Indeed, the medium is kept homogeneous by an efficient low stirring rate of 50 rpm. An approach based on heat convection was described by Wong *et al.* to achieve this state, without significant improvements.[26] For the monolayer fabrication, reaching the withdrawal rate limit involves the lowest decrease of the volume fraction, which is remarkable considering its influence on aggregation. The variation of the volume fractions on the number of layers is observed for a constant rate of 3 mm s^{-1} (Fig. 5 and Fig. ESI-5† for a magnified image).

For (A2) and (B1), a good accordance with the equation proposed is still observed. However, for the volume fraction (C1), a slight deviation is indicated by the presence of holes. The fractures could be due to strong deformation of the self-assembly, *i.e.* adhesion with the substrate and also between particles, during the drying phase and the holes seem to be only due to the lack of material, *i.e.* core@shell particles.

In many cases, the monolayer appearance can be improved when U varies from 3 to 4 mm s^{-1}. The experiment (C2) shows a very well-organized coating on large area (Fig. 6).

This last one represents the best set-up conditions that we found to form large monolayers of core@soft shell particles. Moreover, the process time is only 18 s for a coating as large as 20 × 25 mm^2. At the same time, we also reduced the volume fraction which is the source of aggregation defects. In short-term, this method would be broadened to the template-induced colloidal deposition, providing thus a new order of organization.[46]

The presence of polymer shell has a large influence to guarantee a good crystal quality, notably through their adhesive/elastic contribution as described previously (Fig. 1). Indeed, its presence is first observable by a shape change from a spherical to a semi regular polyhedral.[47] The best way to observe the change of shape is to etch the polymer layer with an electron beam. Few seconds permit to generate a white halo and longer application time involves the appearance of the raw spherical silica as illustrated in Fig. 6c. After the total destruction of the polymeric corona, the colloidal silica particles are not so well-organized. The interparticle distance and the array become irregular due to the apparition of cracks. In a sense, this is an indirect proof of the adhesive/elastic soft polymer contributions which counteract the generation and propagation of defects.

Moreover, the adhesive contribution between core@shell particles allows us to decrease the fabrication time. To the best of our knowledge the fastest dip coating process ever developed was based on a high rate limit of 55 μm s^{-1}.[48] Thanks to our specific particle/substrate interactions, we improve the process until we reach a 4000 μm s^{-1} rate for a monolayer fabrication. Moreover just as vital as the crystal structure is the presence of defects in a crystal. Uncontrolled incorporation of defects can easily degrade the optical properties.[49]

Photonic properties

Photons present several advantages over electrons, such as a greater propagation rate, a larger bandwidth available and a

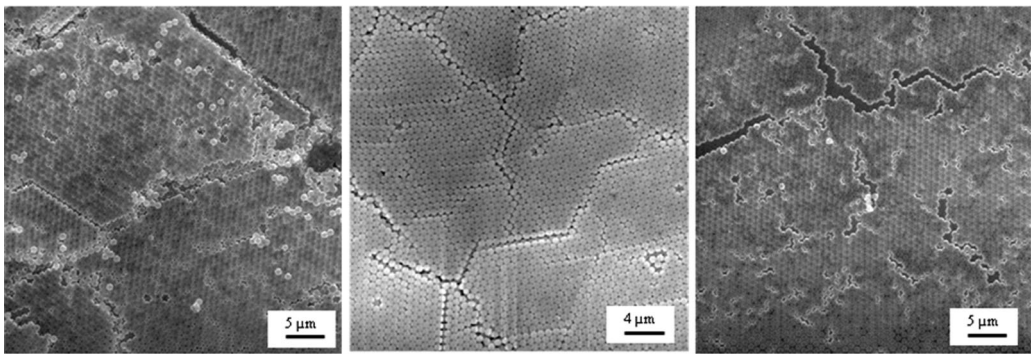

Fig. 5 ESEM observations for 3 mm s^{-1} withdrawal rate for various volume fraction of core@shell silica particles (a) 3 layers with 25 vol% (entry B1 in Table 1) (b) 2 layers with 15 vol% (entry A2 in Table 1) and (c) 1 layer with 3 vol% (entry C1 in Table 1).

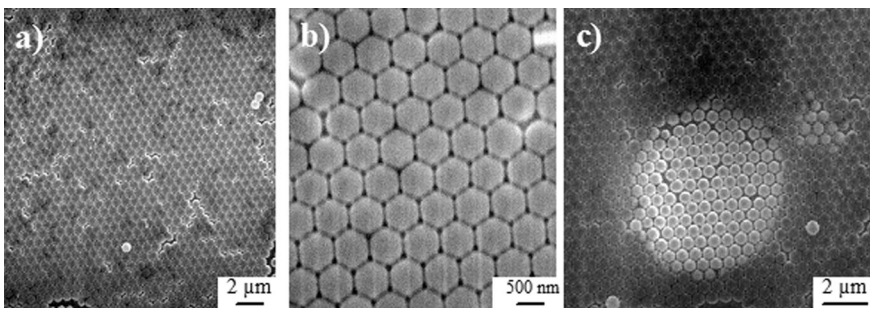

Fig. 6 ESEM images of a monolayer (a,b) before and (c) after electron beam irradiation.

larger information transport. Materials related to the support of photon propagation are called photonic crystals (PCs) or photonic bandgap crystals (PBG). As previously described, these materials consist of a dielectric structure that is periodic in one, two or three dimensions. The dielectric constant or the refractive index periodicity can create a range of forbidden frequencies, so-called photonic bandgap, preventing the photons of the same energy from propagating through the medium. As it has been established, the stacked layers of spherical particles, corresponding to the lattice plane of the *fcc* crystalline structure, act as a diffraction grating for light waves. It can exhibit constructive interferences when Bragg's law is satisfied, *i.e.* similar to X-ray diffraction in crystalline solids.[49,51–55] The most impressive example of such diffractive systems in nature is opals, *i.e.* close-packed amorphous colloidal silica spheres. Consequently, crystalline colloidal arrays can be produced by controlling the size, shape and arrangement of particles, and thus opal-like phenomena with light interactions, also called opalescence, can be obtained as shown in Fig. 7.

Due to the micron size of the core@shell particles and to our specific interest to fabricate and characterize visible light interference phenomena,[50] a goniometric spectroscopy study was performed. Indeed, in classical spectroscopic characterization, *i.e.* in transmission or reflection modes or both, the band gap is expected in the range of 2000 to 2500 nm, corresponding to infrared domain. Herein, the characterization of the synthetic opal photonic properties was lead by a reflection goniometric process. The normal incident visible light ($\beta = 0$) is diffracted into several discrete directions by the opal array (Fig. ESI-1 in electronic supporting information†). In accordance with other experiments, we expected a diffraction of the *fcc* (111) plane and thus a variation of the diffracted wavelength with the Bragg's angle (θ) defined as the angle

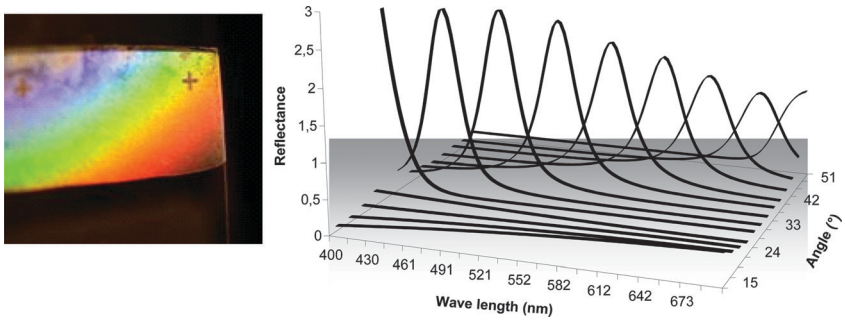

Fig. 7 Optical iridescence of 1 μm core@shell monolayer array of a synthetic opal-like material (left) and positive first order visible diffraction of 1 μm silica core (right).

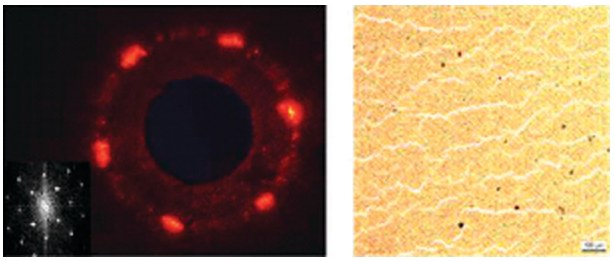

Fig. 8 Laser diffraction pattern and ESEM Fourier Transform of the associated colloidal crystal (inset bottom left), and optical image of a monolayer on large area of 1 mm^2 (scale bar = 100 μm).

between the diffracted beam and the crystallographic plane.[49–53] In the same time, an increasing of the array was expected by narrowing the wavelength extinction with the number of layers. Nevertheless, the spectroscopic data diverge from the predicted ones. Firstly, the diffracted intensity was not influenced by the number of layers but essentially by the homogeneity of the surface. Secondly, the diffraction figure was not effective between two (111) planes but in the plane (111). Indeed, to obtain constructive interference, the phase shifts have to be calculated from two objects belonging to the same plane (2D) and have to be proportional to a multiple of the diffracted wavelength. The main formula which is a purely a geometrical law is then described below (eqn (5)),

$$dn\left(\sin\beta + \sin\left(\frac{\pi}{2} - \theta\right)\right) = \pm m\lambda_0 \qquad (5)$$

where d is the spacing between two consecutive diffracting objects, β is the incident angle, θ the diffracted angle, m the diffraction order, λ_0 the diffracted wavelength in vacuum and n the refractive index of the propagating medium ($n = 1$ for reflection in air).

The core@shell colloidal silica coatings, characterized by goniometric spectroscopy, can be assembled to a 2D grating formed by a regular C6 pattern which diffracts light into several directions, even for 3 to 8 coated layers (Fig. ESI-7 in electronic supporting information†). The surface quality and the array size defined its efficiency, and those are independent of the number of layers.

Moreover, as described in the literature, the 2D diffraction figure can be viewable by a laser transmission experiment[24,52,56] which permits to characterize the C6 pattern symmetry on a large area of few mm^2 (size of the laser spot). This last one can also be correlated to the Fourier Transform (FT) of the ESEM image (Fig. 8).

The presence of the six well-defined spots is characteristic of a well-ordered and oriented colloidal crystal. Indeed, the diffraction figure corresponds to a *hcp* array with the domains oriented in the same direction over the large area of the laser spot. Concerning the influence of the shell thickness on the diffraction behavior, we compared two mono-layers coating with 10 nm and 54 nm polymer thicknesses on 1 μm silica core and no significant variation of behavior has been observed. In this range of thickness, the size of the dense shell does not seem to have any influence on optical properties in dry state.

Conclusions

We have developed an easy and rapid fabrication of well ordered colloidal crystal over large area. The main enhancement is based on the dip coating of adhesive core@shell particles. Sticky in air and hard spheres in solvent, the hybrid Si@PBuA particles present the abilities to self-assemble quickly. Generally produced at 1 μm s^{-1}, the system developed with an organic solvent NPY, with a high boiling point, is able to decrease drastically the processing time due to a large increase of the withdrawal rate towards 4000 μm s^{-1}. Based on a Landau-Levich equation, we proposed a simple model to predict the number of layers, which was controlled experimentally by tuning of the withdrawal rate and the volume fraction.

The accurate control of the number of layers holds for up to a maximum of 18 vol% fraction and a maximum rate of 4000 μm s^{-1}. Above these values, a dewetting of the meniscus is observed and sedimentation appears, creating defects on the coating surface. We established that the inter-particle interactions between hybrid core@soft shell act as adhesive bridges. These bridges support the stability of the colloidal crystal arrays on the inter-particle interface by dissipating the strong repulsion energy and reducing the number of defects.

In addition, we characterized the iridescence of such a grating. An angular analysis confirmed the 2D diffraction evolving with the particle diameter and the crystallographic structure. We have demonstrated the direct relation between the size of the core@shell particles and the photonic properties. Moreover, the goniometric technique permitted us to determine the quality of the self-ordered arrays by the optical detection of the defects. The polymer shell thickness does not influence the photonic behavior until total filling of the spaces between the pores. Indeed, in this latter case, the iridescence stops due to homogeneity of the refractive indexes between the ordered hybrid particles and the continuous medium, leading to the closing of the photonic gap.

Acknowledgements

The authors would like to thank the CNRS for the PhD financial support of the C. Deleuze. Arkema is also acknowledged for the generous donation of the BlocBuilder® initiator. V. Pellerin, M.H. Delville, G. Clisson and A. Khoukh are thanked for their contribution to the chemistry characterizations by ESEM, TEM, SEC and NMR, respectively.

References

1 G. M. Whitesides and B. Grzybowski, *Science*, 2002, **295**, 2418.
2 (*a*) E. Yablonovitch, *Phys. Rev. Lett.*, 1987, **58**, 2059; (*b*) S. John, *Phys. Rev. Lett.*, 1987, **58**, 2486.
3 (*a*) J. H. Holtz and S. A. Asher, *Nature*, 1997, **389**, 829; (*b*) K. Lee and S. A. Asher, *J. Am. Chem. Soc.*, 2000, **122**, 9534.
4 E. Özbay, E. Michel, G. Tuttle, R. Biswas, M. M. Sigalas and K.-M. Ho, *Appl. Phys. Lett.*, 1994, **64**, 2059.
5 N. M. Litchinitser, A. K. Abeeluck, C. Headley and B. J. Eggleton, *Opt. Lett.*, 2002, **27**, 1592.
6 C. E. Reese, A. V. Mikhonin, M. Kamenjicki, A. Tikhonov and S. A. Asher, *J. Am. Chem. Soc.*, 2004, **126**, 1493.
7 S.-Y. Lin, E. Chow, V. Hietala, P. R. Villeneuve and J. D. Joannopoulos, *Science*, 1998, **282**, 274.
8 A. Stein, F. Li and N. R. Denny, *Chem. Mater.*, 2008, **20**, 649.

9 B. D. Gates, Q. Xu, M. Stewart, D. Ryan, C. G. Willson and G. M. Whitesides, *Chem. Rev.*, 2005, **105**, 1171.
10 (*a*) J. G. Fleming and S.-Y. Lin, *Opt. Lett.*, 1999, **24**, 49; (*b*) D. G. Flagello, B. Arnold, S. Hansen, M. Dusa, R. Socha, J. Mulkens and R. Garreis, *Proceedings of SPIE-The International Society for Optical Engineering*, 2004, **5377**(PART 1), 21; (*c*) I. Divliansky, T. S. Mayer, K. S. Holliday and V. H. Crespi, *Appl. Phys. Lett.*, 2003, **82**, 1667.
11 M. Campbell, D. N. Sharp, M. T. Harrison, R. G. Denning and A. J. Turberfield, *Nature*, 2000, **404**, 53.
12 S. Franssila, *Introduction to Microfabrication*, John Wiley & Sons, Inc., 2004, vol. 1.
13 S. P. Murarka, *Mater. Sci. Eng.*, 1998, **19**, 87.
14 F. García-Santamaría, H. T. Miyazaki, A. Urquía, M. Ibisate, M. Belmonte, N. Shinya, F. Meseguer and C. Lopez, *Adv. Mater.*, 2002, **14**, 1144.
15 Y. Xia, B. Gates, Y. Yin and Y. Lu, *Adv. Mater.*, 2000, **12**, 693.
16 A. N. Shipway, E. Katz and I. Willner, *ChemPhysChem*, 2000, **1**, 18.
17 R. Mayoral, J. Requena, J. S. Moya, C. Lopez, A. Cintas, H. Miguez, F. Meseguer, L. Vázquez, M. Holgado and A. Blanco, *Adv. Mater.*, 1997, **9**, 257.
18 K. Ohno, T. Morinaga, S. Takeno, Y. Tsujii and T. Fukuda, *Macromolecules*, 2007, **40**, 9143.
19 A. Van Blaaderen, R. Ruel and P. Wiltzius, *Nature*, 1997, **385**, 321.
20 (*a*) B. Gates, D. Qin and Y. Xia, *Adv. Mater.*, 1999, **11**, 466; (*b*) W. D. Ristenpart, I. A. Aksay and D. A. Saville, *Phys. Rev. Lett.*, 2003, **90**, 128303.
21 P. Jiang and M. J. McFarland, *J. Am. Chem. Soc.*, 2004, **126**, 13778.
22 A. S. Dimitrov and K. Nagayama, *Langmuir*, 1996, **12**, 1303.
23 (*a*) S. Reculusa and S. Ravaine, *Chem. Mater.*, 2003, **15**, 598; (*b*) S. Reculusa, P. Masse and S. Ravaine, *J. Colloid Interface Sci.*, 2004, **279**, 471.
24 P. Jiang, J. F. Bertone, K. S. Hwang and V. L. Colvin, *Chem. Mater.*, 1999, **11**, 2132.
25 R. G. Shimmin, A. J. DiMauro and P. V. Braun, *Langmuir*, 2006, **22**, 6507.
26 S. Wong, V. Kitaev and G. A. Ozin, *J. Am. Chem. Soc.*, 2003, **125**, 15589.
27 L. K. The, N. K. Tan, C. C. Wong and S. Li, *Appl. Phys. A: Mater. Sci. Process.*, 2005, **81**, 1399.
28 G. Lozano and H. Miguez, *Langmuir*, 2007, **23**, 9933.
29 H. F. Payne, *Ind. Eng. Chem.*, 1943, 15.
30 W. Stöber, A. Fink and E. J. Bohn, *J. Colloid Interface Sci.*, 1968, **26**, 6211.
31 (*a*) Z.-Z. Gu, A. Fujishima and O. Sato, *Chem. Mater.*, 2002, **14**, 760; (*b*) J. Ye, R. Zentel, S. Arpiainen, J. Ahopelto, F. Jonsson, S. G. Romanov, Sotomayor and C. M. Torres, *Langmuir*, 2006, **22**, 7378.
32 K. Nozawa, H. Gailhanou, L. Raison, P. Panizza, H. Ushiki, E. Sellier, J. P. Delville and M. H. Delville, *Langmuir*, 2005, **21**, 1516.
33 (*a*) R. Inoubli, S. Dagréou, F. Roby, A. Khoukh, J. Peyrelasse and L. Billon, *Polymer*, 2005, **46**, 2486; (*b*) R. Inoubli, S. Dagreou, A. Lapp, L. Billon and J. Peyrelasse, *Langmuir*, 2006, **22**, 6683; (*c*) R. Inoubli, S. Dagréou, M. H. Delville, A. Lapp, J. Peyrelasse and L. Billon, *Soft Matter*, 2007, **3**, 1014.
34 C. Deleuze, M. H. Delville, V. Pellerin, C. Derail and L. Billon, *Macromolecules*, 2009, **42**, 5303.
35 (*a*) J. Parvole, G. Laruelle, A. Khoukh and L. Billon, *Macromol. Chem. Phys.*, 2005, **206**, 372; (*b*) J. Parvole, J. P. Montfort and L. Billon, *Macromol. Chem. Phys.*, 2004, **205**, 1369.
36 N. Jullian, F. Leonardi, B. Grassl, J. Peyrelasse and C. Derail, *Appl. Rheol.*, 2010, **20**, 33685.
37 (*a*) I. Borukhov and L. Leibler, *Macromolecules*, 2002, **35**(13), 5171; (*b*) K. R. Shull, K. I. Winey, E. L. Thomas and E. J. Kramer, *Macromolecules*, 2001, **24**, 2748.
38 A. Zosel, *Int. J. Adhes. Adhes.*, 1998, **18**, 265.
39 B. V. Derjaguin, V. M. Muller and P. Yu. Toporov, *J. Colloid Interface Sci.*, 1975, **53**, 314.
40 (*a*) M. H. Kim, H. K. Choi, O. O. Park and S. H. Im, *Appl. Phys. Lett.*, 2006, **88**, 143127; (*b*) H. K. Choi, M. H. Kim, S. H. Im and O. O. Park, *Adv. Funct. Mater.*, 2009, **19**, 1.
41 Y. Masuda, T. Itoh, M. Itoh and K. Koumoto, *Langmuir*, 2004, **20**, 5588.
42 L. V. Woodcock, *Nature*, 1997, **385**, 141.
43 L. Meng, H. Wei, A. Nagel, B. J. Wiley, L. E. Scriven and D. J. Norris, *Nano Lett.*, 2006, **6**, 2249.
44 S. H. Im, M. H. Kim and O. O. Park, *Chem. Mater.*, 2002, **15**, 1797.
45 P. Masse, G. Pouclet and S. Ravaine, *Adv. Mater.*, 2008, **20**, 584.
46 J. P. Hoogenboom, C. Rétif, E. De Bres, M. Van De Boer, A. K. Van Langen-Suurling, J. Romijn and A. Van Blaaderen, *Nano Lett.*, 2004, **4**, 205.
47 J. L. Keddie, *Mater. Sci. Eng., R*, 1997, **21**, 101.
48 M. H. Kim, S. H. Im and O. O. Park, *Adv. Funct. Mater.*, 2005, **15**, 1329.
49 Y. A. Vlasov, V. N. Astratov, A. V. Baryshev, A. A. Kaplyanskii, O. Z. Karimov and M. F. Limonov, *Phys. Rev. E: Stat. Phys., Plasmas, Fluids, Relat. Interdiscip. Top.*, 2000, **61**(5), 5784.
50 (*a*) L. Ghannam, H. Garay, M. Bacou, J. Francois, M. E. R. Shanahan and L. Billon, *Polymer*, 2004, **45**, 7035; (*b*) L. Ghannam, H. Garay, J. Francois, M. E. R. Shanahan and L. Billon, *Chem. Mater.*, 2005, **17**, 3837; (*c*) L. Ghannam, H. Garay, J. Francois and L. Billon, *Macromol. Chem. Phys.*, 2007, **208**, 1469; (*d*) L. Ghannam, H. Garay and L. Billon, *Macromolecules*, 2008, **41**, 7374; (*e*) M. Joubert, A. Khoukh, J. F. Tranchant, F. Morvan and L. Billon, *Macromol. Chem. Phys.*, 2009, **210**, 1542.
51 S. A. Asher, J. M. Weissman, A. Tikhonov, R. D. Coalson and R. Kesavamoorthy, *Phys. Rev. E: Stat., Nonlinear, Soft Matter Phys.*, 2004, **69**, 1.
52 L. M. Goldenberg, J. Wagner, J. Stumpe, B.-R. Paulke and E. Görnitz, *Langmuir*, 2002, **18**, 3319.
53 H. Miguez, F. Meseguer, C. Lopez, A. Mifsud, J. S. Moya and L. Vazquez, *Langmuir*, 1997, **13**, 6009.
54 H. Miguez, C. Lopez, F. Meseguer, A. Blanco, L. Vazquez, R. Mayoral, M. Ocana, V. Fornes and A. Mifsud, *Appl. Phys. Lett.*, 1997, **71**, 1148.
55 J. F. Dechezelles, T. Aubert, F. Grasset, S. Cordier, C. Barthou, C. Schwob, A. Maitre, R. Vallee, H. Cramail and S. Ravaine, *Phys. Chem. Chem. Phys.*, 2010, **12**, 11993.
56 L. Billon, M. Manguian, V. Pellerin, M. Joubert, O. Eterradossi and H. Garay, *Macromolecules*, 2009, **42**, 345.